24th COBEM - 2017

24th ABCM International Congress of Mechanical Engineering
December 3-8, 2017, Curitiba, PR, Brazil

COBEM-2017-1122
HIGH STRAIN-RATE BEHAVIOR OF FIBER-REINFORCED THERMOPLASTIC COMPOSITES UNDER COMPRESSIVE LOADINGS

Carolina Ramírez Montes
Universidad Autónoma de Nuevo León, Facultad de Ingeniería Mecánica y Eléctrica, Centro de Investigación e Innovación en Ingeniería Aeronáutica
caroramirezmontes@gmail.com

Vitor Luiz Reis
Carlos Vinicios Opelt
Instituto Tecnológico de Aeronáutica
vreis88@gmail.com, cvopelt@gmail.com

Rafael Celeghini Santiago
Universidade Federal do ABC, Centro de Engenharia, Modelagem e Ciências Sociais Aplicadas - CECS
rafael.santiago@ufabc.edu.br

Maribel C Rezende
Universidade Federal do Estado de São Paulo
mirabelcr@gmail.com

Citlalli Gaona Tiburcio
Universidad Autónoma de Nuevo León, Facultad de Ingeniería Mecánica y Eléctrica, Centro de Investigación e Innovación en Ingeniería Aeronáutica
citalli.gaona@gmail.com

Maurício Vicente Donadon
Instituto Tecnológico de Aeronáutica
donadon@ita.br

Abstract. *This work presents an experimental study on the mechanical behavior of polyphenylene sulfide (PPS) based composite laminates reinforced with carbon and glass fibers, subjected to high strain rates under compression load. The specimens were tested using a Split Hopkinson Pressure Bar (SHPB) testing apparatus and an electromechanical universal testing machine for dynamic and quasi-static regimen, respectively. High speed imaging system was used to monitor the failure process during the tests and fractography analysis was performed to identify and understand the influence of the strain rate on the damage mechanisms. Results showed that mechanical properties of PPS carbon fiber-reinforced composite (CF/PPS) are not strain rate dependent, but mechanical properties of PPS glass fiber-reinforced composite (GF/PPS) are strain rate dependent. All the specimens tested exhibited a failure caused by the joint effect of out-of-plane shear and delamination.*

Keywords: *Fiber-reinforced thermoplastic composites, high strain rate, Split Hopkinson Pressure Bar*

1. INTRODUCTION

A composite material is the combination of two or more constituents with significantly different macroscopic behavior and a distinct interface between each constituent (on the microscopic level), their main purpose is getting a combination of properties that is not possible to obtain in the original materials (Staab, 2015). Fiber-reinforced polymer composites (FRPC) are materials which are composed of fibers made of glass, aramid, carbon, boron or silicon carbide; embedded in a polymeric matrix (thermoplastic or thermoset resins) (Gay *et al.*, 2003; Mallick, 2007). The ability to tailor mechanical properties of FRPC according to fiber orientation and matrix type makes them the most used composites in structural applications in different fields like armor, aerospace, automotive, marine, civil engineering

structures, sports goods, etc. taking advantage of their high specific strength, specific stiffness and strength to weight ratios, good corrosion resistance and improved fatigue properties (Hosur *et al.*, 2003).

Special properties like low-cost rapid manufacturing with low cycle times that allow for medium to high volume production, capability of complex geometry through an injection molding process, recyclability, better damage tolerance (impact toughness), fire/smoke/toxicity performance, chemical resistance and near-infinitive shelf life at room temperature have made thermoplastic composite more attractive compared with thermoset materials, which has increased its use, especially in aerospace structures (Leeser, 2010; Red, 2014; Soutis, 2015; TenCate, 2016; Vodicka, 1996). These structures may be subjected to dynamic loads like impact with foreign objects, projectile impacts or shock waves which produce large deformation in the material in fractions of millisecond, however, in absence of totally understanding of high strain rates effects on FRPC behavior, static properties have been used for material selection and design, which could lead to conservative estimates as excessive weight design or unexplained and untimely failure. Moreover, the development of constitutive equations for the composite material used in structures subjected to dynamic loads to predict their performance using finite element modeling (FEM), among others, requires the knowledge of how the strength, strain and failure mode vary with the strain rate, what makes essential the characterization of the material's response in such loading regime (Fitoussi *et al.*, 2012; Hamouda and Hashmi, 1998; Hosur *et al.*, 2003; Jadhav, 2003).

Some researchers have reported, in the open literature, results on the mechanical behavior of FRPC at high strain rates (with different types of loading – compressive, tensile, shear and multiaxial loading) and its relationship with the configuration of the material, i.e. type of resin and type, length, concentration and orientation of fibers (Nemat-Nasser, 2000). Nevertheless, most of these studies are about thermoset composites, specially epoxy and polyester matrices reinforced with glass and carbon fibers (Barré *et al.*, 1996; Hamouda and Hashmi, 1998; Jacob *et al.*, 2004), with just a few works focused on thermoplastic composites. Among the studies on thermoplastic composites submitted to high strain rates, it can be cite polyamide reinforced composites (with glass and carbon fiber with different fiber configurations), ethylene-propylene copolymer (EPC) matrix reinforced with discontinuous glass fibers, commingled e-glass/polypropylene woven fabric composite, glass-fiber reinforced polypropylene (PP) and polybutene-1 (PB-1) and AS4 graphite/PEEK thermoplastic composite; and none about PPS matrix composites (Brown *et al.*, 2010; Fitoussi *et al.*, 2012; Jendli *et al.*, 2014; Montiel and Williams, 1990; Ploeckl *et al.*, 2015; SchoBig *et al.*, 2008; Todo *et al.*, 2000; Weeks and Sun, 1998).

Within this context, the present research focuses on an experimental characterization of strain rate effect on the mechanical behavior under compression loading of a CF/PPS and GF/PPS using a Split Hopkinson Pressure Bar apparatus for dynamic test and electromechanical universal testing machine for quasi-static regimen. Additionally, fractography analyses are also performed in order to identify the influence of the strain rate on the damage mechanisms of the material.

2. EXPERIMENTAL PROCEDURE

2.1 Material Description

The material used in this study was provided by TenCate in form of rectangular laminates in two versions:

a) 33 plies thick laminate consisting of carbon fabric, 5HS style (harness-satin weave, Fig. 1a), 3K (three thousand individual strands of carbon per fiber bundle) T300J (Toray Carbon Fibers America, Inc specification, commonly used in aerospace applications), 280 gsm FAW (fiber area weight in grams per square meter), combined with 42% RC (resin content by weight) Fortron 214 PPS in an orthotropic [0°/90°]s balanced/mirrored lay-up;

b) 42 plies thick laminate consisting of fiber glass fabric, 8HS style (harness-satin weave Fig. 1b), EC6 yarn (e-glass continuous fiber with filament diameter 6 microns), 300 gsm FAW, combined with 33% RC Fortron 214 PPS in an orthotropic [0°/90°]s balanced/mirrored lay-up.

Figure 1. Harness-satin weave (a) 5HS, (b) 8HS (ACP Composites, 2017).

Rectangular specimens of 9x10 mm^2 (width x length) were cut from the originals laminates using the Extec Labcut 5000 which guarantees samples with parallel tolerance of 0.03 mm. The height of the specimen is the same thickness of the original laminate, 9.8 mm for carbon fiber and 10 mm for glass fiber (Fig. 2). The geometry of the specimens was set between the ranges specified to accomplish the assumptions made about inertia and friction effect during SHPB tests (Gama *et al.*, 2004). The load was applied in the longitudinal direction which coincides with the warp direction (Fig. 2). Three specimens were tested at each strain rate.

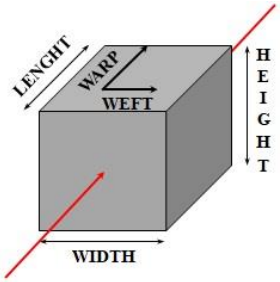

Figure 2. Isometric view of the specimen.

2.2 Quasi-static tests

Quasi-static reference tests were performed using an INSTRON servo-mechanic universal testing machine (Fig. 3a) at three constant displacement rates (0.6, 6 and 60 mm/min), which corresponds to three quasi-static axial strain rates 0.001, 0.01 and 0.1 s^{-1} by considering the nominal specimen length of 10 mm. Load measurements were recorded using universal testing machine hardware and software. An Imetrum video gauge system synchronized with the testing machine was used to measure strain in the specimen. Using the software interface target points were placed at the center of the specimen and the strain measurements were recorded during the test. Figure 3b shows loading configuration used in the quasi-static tests. Special plates, with load distribution system in the movable head member, were used to apply the load to the specimen.

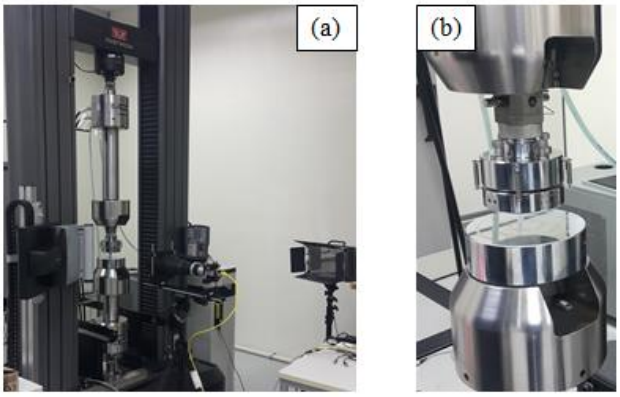

Figure 3. (a) Instron testing machine and Imetrum system assembly and (b) Test jig used in the quasi-static compression tests.

2.3 Dynamic test

High strain rate tests were performed using a Split Hopkinson Pressure Bar apparatus available in the Aerospace Structures Laboratory at Instituto Tecnológico de Aeronáutica (ITA). Details about the testing apparatus and data reduction schemes used to compute strain, stress and strain rates in the specimen can be found in Reis et al. (2015). Additionally, a Photron High Speed Imaging System (HSIS) composed of a high speed camera model FASTCAM SA-Z and FASTCAM analysis software was set up with the SHPB apparatus to capture videos and images during the experiments. Figure 4 shows the SHPB testing setup used for the dynamic tests.

Figure 4. SPHB apparatus and HISIS set up.

In a traditional compression SHPB test, a specimen is sandwiched between an incident bar and a transmitted bar (Fig. 5). Striker is accelerated by a gas gun up to an initial velocity (V_0) impacting the free edge of the incident bar, this produces an elastic compressive pulse with almost rectangular shape and amplitude proportional to the impact velocity of the striker bar. The pulse travels along the incident bar and is recorded by a pair of diametrically opposed gages placed in the middle of the incident bar ($\varepsilon_i(t)$). On the incident bar-specimen interface a part of the wave is reflected ($\varepsilon_r(t)$); and part of it propagates through the specimen and to the transmitted bar where another pair of diametrically opposed gages are placed on and record that signal ($\varepsilon_t(t)$). These signals were post-processed using an in-house Phyton program, which computes the stress, strain and strain rate on the specimen using the classical SHPB analysis based on the one dimensional wave propagation theory (Chen and Song, 2011; Gama et al., 2004; Gray III, 2000; Ploeckl et al., 2015; Reis et al., 2015).

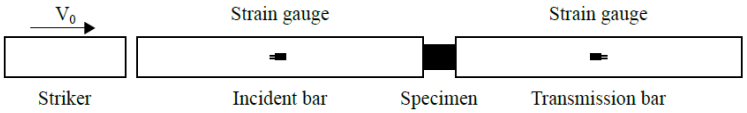

Figure 5. Schematic view of SHPB test (Reis et al., 2015)

Several assumptions must be made to obtain accurate measurements from the SHPB set up when the one dimensional wave propagation theory is applied, these imply elastic deformation in the bars during the test, unidirectional elastic pulses propagate along the bars, uniform ddeformation process in the specimen, no dispersion of waves throughout the bars ans the specimen. The stress inside the specimen (σ_S) is calculated assuming dynamic equilibrium developed at the bar ends in contact with the sample, by Eq. (1) where E is the Young's modulus of the bars, A y A_S are the cross-sectional areas of the bars and the specimen, respectively. The specimen strain is calculated Eq. (2) while tha strain rate is obtained by Eq. (3).

$$\sigma_S(t) = \frac{1}{2}\frac{P_1(t)+P_2(t)}{A_S} = \frac{EA}{2A_S}(\varepsilon_i(t)+\varepsilon_r(t)+\varepsilon_t(t)) \tag{1}$$

$$\varepsilon_S(t) = \frac{c_O}{L_S}\int_0^t(\varepsilon_i(t)-\varepsilon_r(t)-\varepsilon_t(t))dt \tag{2}$$

$$\dot{\varepsilon}_S(t) = \frac{c_O}{L_S}(\varepsilon_i(t)-\varepsilon_r(t)-\varepsilon_t(t)) \tag{3}$$

where $c_O = \sqrt{E/\rho}$ is the speed of elastic wave, ρ is the desity of the bars amd L_S is the length of the specimen (Chen and Song, 2011; Gama et al., 2004; Gray III, 2000; Ploeckl et al., 2015; Reis et al., 2015)..

Two pressure values were set in the gas chamber (1.2 and 1.6 bar), establishing two strain rates to characterize the materials behavior in the dynamic regime.

3. RESULTS

3.1 PPS Carbon fiber-reinforced composite

Quasi-static and dynamic tests were performed until failure at 0.001, 0.01, 0.1 400.5 and 832.3 s^{-1}. Figure 6a shows forces equilibrium plot achieved during dynamic tests where the red line is the force in the incident bar/specimen interface and the blue line is the force in the specimen/transmitted bar interface, the tendency exhibited means that the measurements realized with the SHPB apparatus are correct. Figure 6b shows the longitudinal compressive stress-strain

(σ-ε) curves for the material. Young's modulus was calculated as the slope of the lineal curve obtained in the range of strain values of 0.7% - 1.5%. Table 1 summarizes the average values of the results obtained in each tested strain rate together with the standard deviation (STDV) and coefficient of variation (CV).

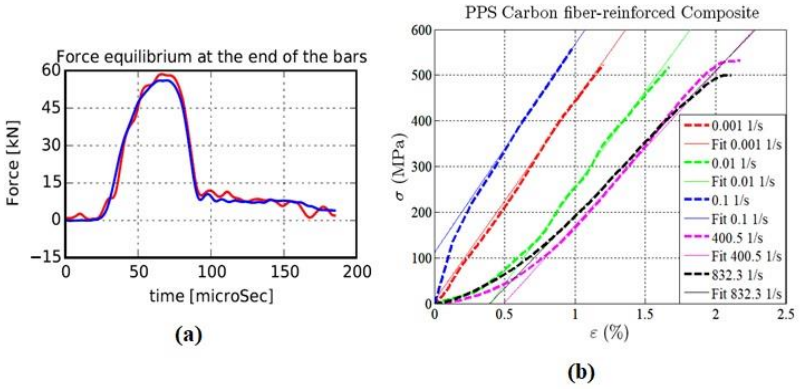

Figure 6. (a) Forces equilibrium graph during dynamic tests at 832.3 s^{-1} and (b) Quasi-static and dynamic stress-strain curves, obtained for CF/PPS.

Table 1. Experimental results for CF/PPS tested in the quasi-static and dynamic regimes.

$\dot{\varepsilon}$ (s^{-1})	σ_{PEAK} (MPa)	$\varepsilon_{\sigma_{PEAK}}$ (%)	E (GPa)
0.001	521.926	1.203	43.664
0.01	517.869	1.67	42.271
0.1	558.013	0.978	45.643
400.5	525.747	2.148	35.493
832.3	534.726	2.134	33.053
Average	531.656	1.627	40.025
STDV	14.309	0.475	4.878
CV (%)	2.691	29.2305	12.189

The results indicate that the composite strength remains constant while ultimate strain increases with the strain rate. The increase in strain with the strain rate for the same stress level is reflected in the Young's modulus reduction with increasing strain rates. Figure 7 shows plots of the failure stress, ultimate strain and material Young's modulus versus strain rate.

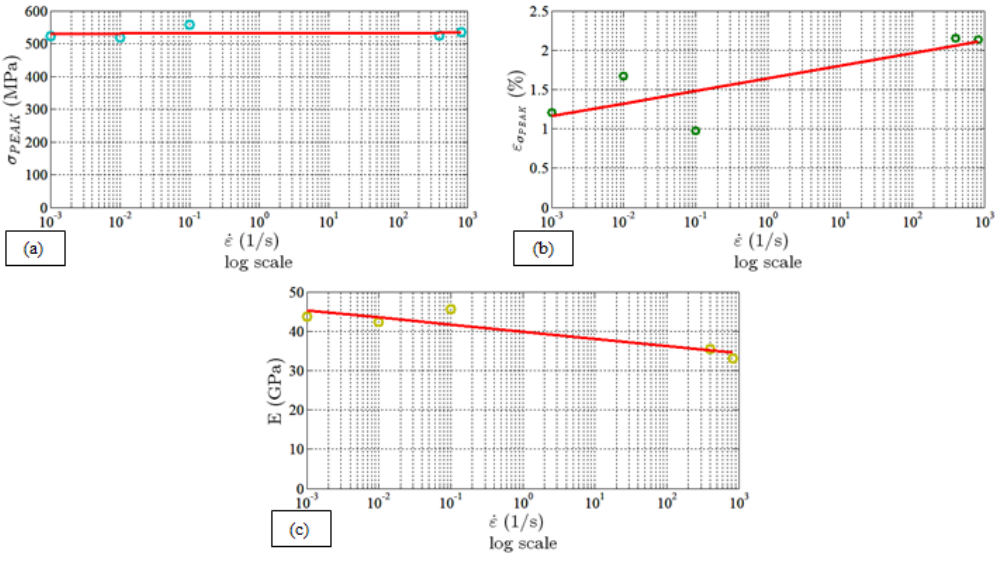

Figure 7. CF/PPS properties as function of the strain rate (a) stenght - strain rate plot, (b) ultimate strain – strain rate plot and (c) Young Modulus – strain rate plot.

All tested specimens showed signs of shear damages and delaminations, respectively pointed as yellow and red arrows. This kind of damages is a direct result of the fiber architecture used, namely 5 harness satin weave. The fiber waviness of the textile promotes the occurrence of shear planes, which lead to the out of plane shear damages (through-the-thickness). At the same time, the fiber interweaving inhibits the propagations of failures inside the layers (intralaminar failures). Therefore, less fracture energy is required for the cracks to propagation as interlaminar failures, i.e. delaminations (Greenhalgh, 2009). Some specimens tested in quasi-static loading conditions exhibited local kink-bands, as seen in Fig. 8a and b. The kink-bands are recognized as one of the main compressive failure mechanisms, and its occurrence is usually related to some degree of fiber misalignment (Opelt, 2017). For higher strain rates, the composite material does not have sufficient time to properly accommodate the imposed deformation, which ends up suppressing the occurrence of kink-bands.

Specimens loaded at high strain rate were split into several pieces, which was most likely caused by the viscoelastic nature of the polymer matrix. At higher strain rates the behavior of the polymer matrix becomes more brittle and, thus, prone to exhibit delaminations. The occurrence of multiple delaminations in the early stage of failure could then result in the fragmentation into several pieces. As seen in Fig. 9a, the surface of some fragments exhibited aspects very similar to wear damages in polymers (Bertholdi et al., 2014; dos Santos et al., 2013). These wear damages could be a result of the rapid delamination growth, which promote the friction between the delaminated parts.

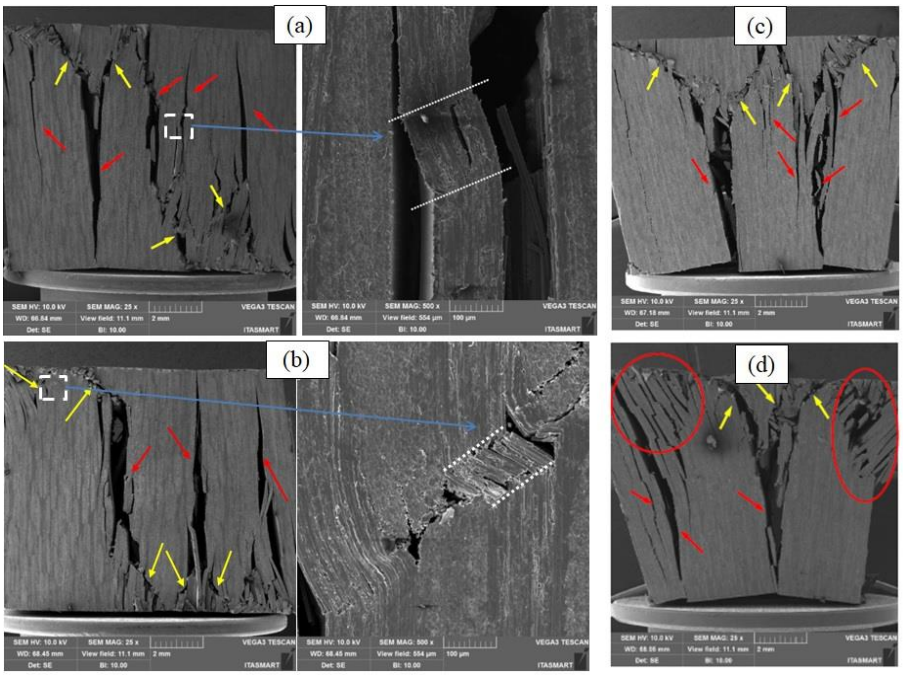

Figure 8. Quasi-static failure modes observation using SEM for CF/PPS (a) 0.001 s^{-1} at 25X with an amplified zone at 500X to show kink band formation, (b) 0.01 s^{-1} with an amplified zone at 500X to show kink band, (c) 0.1 s^{-1} at 25X, and (d) 400.5 s^{-1} at 25X. Shear failure mode in yellow and delamination in red.

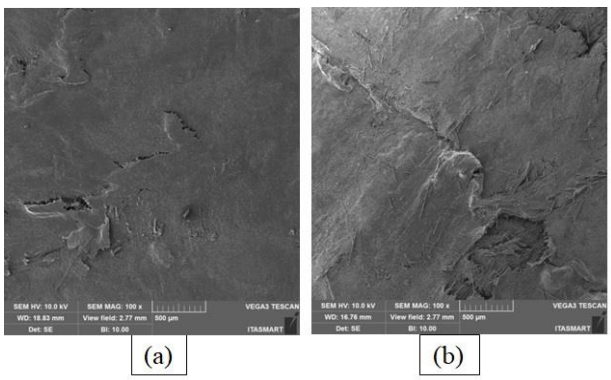

Figure 9. SEM images of fracture surface of (a) CF/PPS specimen tested at 832.3 s^{-1} (100X), and (b) GF/PPS specimen tested at 891.1 s^{-1} (100X).

3.2 PPS Glass fiber-reinforced composite

Figure 10a shows forces equilibrium plot achieved during dynamic tests for GF/PPS, where the red line is the force in the incident bar/specimen interface and the blue line is the force in the specimen/transmitted bar interface, the tendency exhibited means that the measurements realized with the SHPB apparatus are correct. Figure 10b shows stress-strain curves for GF/PPS tested at quasi-static and dynamic regimes. The dynamic tests resulted in strain rates of 558.5 and 891.1 s^{-1} at the two pressure values established before (1.2 and 1.6 bar). The tested specimens exhibited a fairly linear stress-strain behavior up to failure where no significant changes in the Young's modulus with increasing strain rates were observed. Young's modulus was calculated as the slope of the lineal curve obtained in the range of strain values of 0.7% - 1.5%. Table 2 summarizes and compares the results obtained for specimen tested at different strain rates in the quasi-static regime.

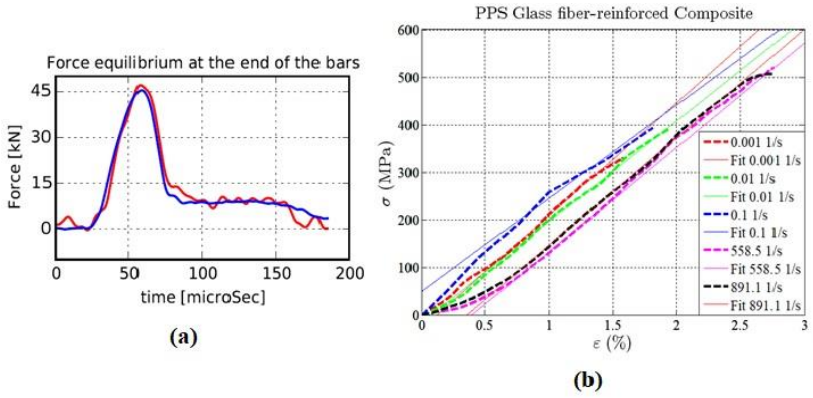

Figure 10. (a) Forces equilibrium graph during dynamic tests at 891.1 s^{-1} and (b) Quasi-static and dynamic stress-strain curves obtained for GF/PPS.

Table 2. Experimental results for GF/PPS specimens tested in the quasi-static regime.

$\dot{\varepsilon}$ (s^{-1})	σ_{PEAK} (MPa)	$\varepsilon_{\sigma_{PEAK}}$ (%)	E (GPa)
0.001	333.421	1.606	22.786
0.01	362.757	1.883	21.79
0.1	378.708	1.539	21.42
Average	358.295	1.676	21.999
STDV	18.756	0.149	0.577
CV (%)	5.2347	8.875	2.623

Table 3. Experimental results for GF/PPS specimens tested in the dynamic regime.

$\dot{\varepsilon}$ (s^{-1})	σ_{PEAK} (MPa)	$\varepsilon_{\sigma_{PEAK}}$ (%)	E (GPa)
558.5	491.886	2.575	22.293
891.1	491.223	2.719	22.703
Average	491.554	2.647	22.498
STDV	0.3316	0.0723	0.205
CV (%)	0.0675	2.732	0.912

The results for specimens tested at different strain rates in the dynamic regime are compared in Tab. 3, where material properties are almost the same in the regime tested. However when results obtained for specimens tested in the quasi-static and dynamic regimes are compared increase on peak stress and failure strain with increasing strain rates stress is observed (Fig. 11). Average strength values of 358.295 MPa and 491.554 MPa were observed for specimens tested in the quasi-static and dynamic regimes, respectively, where a strain rate enhancement of 27% in the strength was observed for the specimens loaded at high strain rates. A similar trend of strength increase was reported by Brown et al. (2010). In the case of ultimate strain (1.676% for quasi-static tests and 2.647% for dynamic tests) a strain rate enhancement of 36% in ultimate strain values was observed for specimens loaded at high strain rates. No significant

changes in the Young's modulus were observed for specimens loaded in the dynamic regime in comparison with those tested in the quasi-static regime.

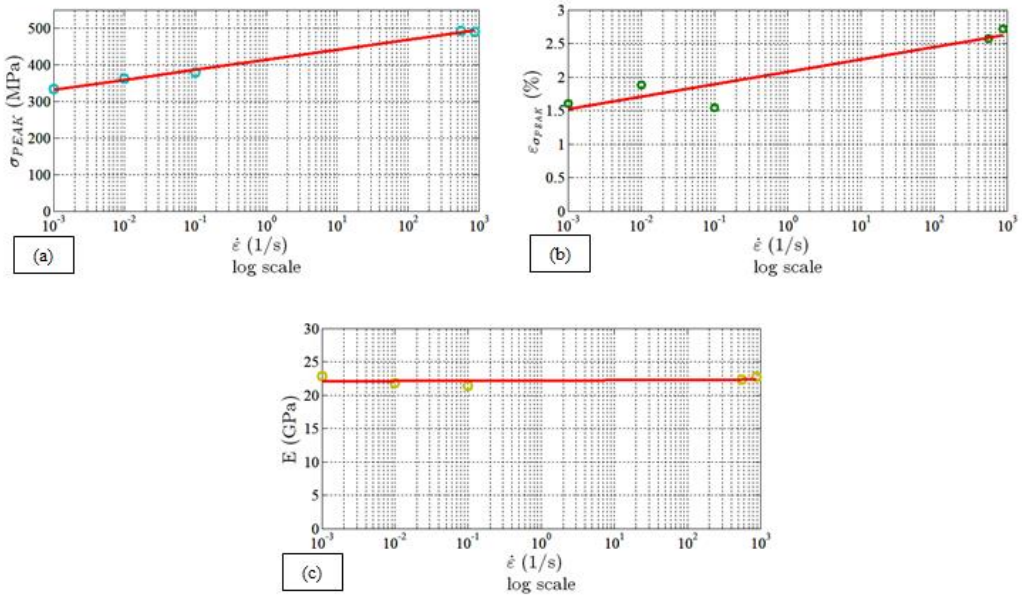

Figure 11. GF/PPS properties behavior related to strain rate (a) peak stress - strain rate graph, (b) strain at peak stress – strain rate graph and (c) Young Modulus – strain rate graph.

The failure of the GF/PPS specimens, seen in Fig.12, was also caused by a joint effect of out of plane shear and delaminations, i.e. a mixed mode failure. Although, here the shear damages are dominant, differently from the CF/PPS specimens, which did not exhibited a dominant failure mode. The GF/PPS specimens submitted to the higher strain rate were also separated into numerous delaminated parts. As for the CF/PPS specimens, here it was possible to identify the aspects of wear damages (Fig. 12b), caused by the friction between the delaminated surfaces. After the tests, was possible to feel a burnt smell. This was likely a result of the degradation of the polymer matrix due to the fast heating caused by the friction, which was confirmed by the darker color of the surface of the parts.

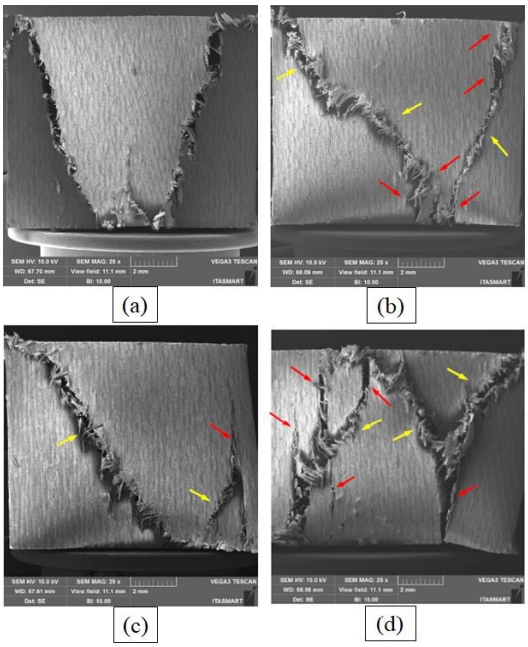

Figure 12. SEM images at 25X of the GF/PPS specimens test at (a) $0.001s^{-1}$, (b) $0.01s^{-1}$, (c) $0.1s^{-1}$ and (d) $558.5s^{-1}$. The failures were moostly caused by out-of-plane shear (yellow arrows) with some degree of delamination growth (red arrows).

4. CONCLUSIONS

The effect of strain rate over mechanical properties of two thermoplastic fiber reinforced composites was presented in this paper. Results shows that for PPS glass fiber reinforced composite strength and ultimate strain are strain rate dependent. An increase of 27% on peak stress was observed when strain rate is increased from quasi-static to dynamic regime, while strain at peak stress increases about 36%. The strain rate enhancement on mechanical properties is related to the viscoelastic behavior of the polymeric matrix. PPS carbon fiber reinforced composite behavior indicates that strength is not strain rate dependent and remains almost constant white increasing strain rates. This trend indicates that compressive behavior of this material is affected in major proportion by other aspect like fiber-matrix interface and is not just matrix-dominated where fiber is not strain rate dependent.

Mixed failure mode was observed for specimens at low and high strain rates. This behavior implies that the fiber architecture had a greater influence on the fracture process than the strain rate, which results in large occurrence of shear failures. When the specimens were tested using the higher gas pressure (higher strain rate), the delamination growth occurred in the beginning of the fracture process. This caused the specimen to separate into delaminated pieces, which exhibited wear damages due to the friction caused by the rapid delamination growth.

5. REFERENCES

ACP Composites. (2017). Woven Fabric Style Guide | ACP Composites. Retrieved August 8, 2017, from https://store.acpsales.com/products/3495/woven-fabric-style-guide

Barré, S., Chotard, T., & Benzeggagh, M. L. (1996). Comparative study of strain rate effects on mechanical properties of glass fibre-reinforced thermoset matrix composite. *Composites Part A*, *27A*, 1169–1181. https://doi.org/10.1016/1359-835X(96)00075-9

Bertholdi, J., Opelt, C. V., Milan, J. C. G., Coelho, L. A. F., & Lepienski, C. M. (2014). Propriedades mecânicas, tribológicas e térmicas de nanocompósitos de PLLA com nanotubos de carbono de paredes múltiplas. *Polímeros*, *24*(4), 514–520. https://doi.org/10.1590/0104-1428.1313

Brown, K. A., Brooks, R., & Warrior, N. A. (2010). The static and high strain rate behaviour of a commingled E-glass/polypropylene woven fabric composite. *Composites Science and Technology*, *70*, 272–283. https://doi.org/10.1016/j.compscitech.2009.10.018

Cantwell, W. J., & Morton, J. (1991). The impact resistance of composite materials - a review. *Composites*, *22*(5), 347–362. https://doi.org/10.1016/0010-4361(91)90549-V

Chen, W. W., & Song, B. (2011). *Split Hopkison (Kolsky) Bar. Design, Testing and Applications*. New York: Springer.

dos Santos, M. N., Opelt, C. V., Pezzin, S. H., Amico, S. C., Costa, C. E. Da, Milan, J. C., … Coelho, L. A. F. (2013). Nanocomposite of photocurable epoxy-acrylate resin and carbon nanotubes: dynamic-mechanical, thermal and tribological properties. *Materials Research*, *16*(2), 367–374. https://doi.org/10.1590/S1516-14392012005000175

Fitoussi, J., Bocquet, M., & Meraghni, F. (2012). Effect of the matrix behavior on the damage of ethylene-propylene galss fiber reinforced composite subjected to high strain rate tension. *Composites: Part B*, *45*, 1181–1191.

Gama, B. A., Lopatnikov, S. L., & Gillespie Jr, J. W. (2004). Hopkinson bar experimental technique: A critical review. *Applied Mechanics Reviews*, *57*(4), 223–250. https://doi.org/10.1115/1.1704626

Gay, D., Hoa, S. V, & Tsai, S. W. (2003). *Composite Materials Design and Applications*. Boca Raton: CRC Press LLC.

Gray III, G. T. (2000). Classic Split-Hopkinson Pressure Bar Testing. In *ASM Handbook Volume 8 Mechanical Testing and Evaluation*. Ohio: ASM International.

Greenhalgh, E. S. (2009). *Failure analysis and fracture of polymer composites*. *Journal of Chemical Information and Modeling* (Vol. 53). Boca Raton: CRC Press LLC. https://doi.org/10.1017/CBO9781107415324.004

Hamouda, A. M. S., & Hashmi, M. S. J. (1998). Testing of composite materials at high rates of strain: advances and challenges. *Journal of Materials Processing Technology*, *77*, 327–336. https://doi.org/10.1016/S0924-0136(97)00436-6

Hosur, M. V., Alexander, J., Vaidya, U. K., Jeelani, S., & Mayer, A. (2003). High Strain Rate Compression Characterization of Affordable Woven Carbon/Epoxy Composites under off-Axis Loading. *Polymers and Polymer Composites*, *11*(7), 527–539.

Jacob, G. C., Starbuck, J. M., Fellers, J. F., Simunovic, S., & Boeman, R. G. (2004). Strain rate effects on the mechanical properties of polymer composite materials. *Journal of Applied Polymer Science*, *94*, 296–301. https://doi.org/10.1002/app.20901

Jadhav, A. (2003). *High Strain Rate Properties of Polymer Matrix Composites*. Louisiana State University and Agricultural and Mechanical College. Retrieved from http://etd.lsu.edu/docs/available/etd-0708103-114809/

Jendli, Z., Walrick, J.-C., Bocquet, M., & Fitoussi, J. (2014). Strain Rate Effects on the Mechanical Behavior of Carbon-Thermoplastic Matrix Woven Composites. In *ECCM16 - 16th European Conference on Composite Materials*.

Leeser, D. (2010). Thermoplastic Composites , A Proven Composite Material Technology Generates New Interest. Retrieved from http://www.tencate.com/advancedcomposites/products/thermoplastic/default.aspx

Mallick, P. K. (2007). *Fiber-Reinforced Composites Materials, Manufacturing and Design* (Third Edit). Boca Raton: CRC Press Taylor & Francis Group. https://doi.org/10.3144/expresspolymlett.2007.115

Montiel, D. M., & Williams, C. J. (1990). *Method for Evaluating the High Strain-Rate Compressive Properties of Thick Composite Laminates*. Bethesda.

Nemat-Nasser, S. (2000). High Strain Rate Tension and Compression Tests. In *ASM Handbook Volume 8 Mechanical Testing and Evaluation*. Ohio: ASM International. https://doi.org/10.1017/CBO9781107415324.004

Opelt, C. V. (2017). *Estudo dos Modos de Falha em Compressao Uniaxial de Compósitos Avancados: Nova Proposta de Classificacao*. Instituo Tecnológico de Aeronáutica.

Ploeckl, M., Kuhn, P., & Koerber, H. (2015). Characterization of unidirectional carbon fiber reinforced polyamide-6 thermoplastic composite under longitudinal compression loading at high strain rate. *EPJ Web of Conferences*, *94*(1041), 1–6. https://doi.org/10.1051/epjconf/20159401041

Red, C. (2014). The Outlook for Thermoplastics in Aerospace Composites, 2014-2023 : CompositesWorld. Retrieved July 25, 2017, from http://www.compositesworld.com/articles/the-outlook-for-thermoplastics-in-aerospace-composites-2014-2023

Reis, V. L., Marini, L. F., Donadon, M. V., Dutra, T. A., Baldo Junior, J. E., & Nunes de Mello, W. L. (2015). Experimental investigation on the influence of the geometry of carbon fiber specimen used in Split Hopkinson Pressure Bar tests. In *23rd ABCM International Congress of mechanical Engineering*. Rio de Janeiro: Associação Brasileira de Engenharia e Ciências Mecãnicas.

SchoBig, M., Bierögel, C., Grellmann, W., & Mecklenburg, T. (2008). Mechanical behavior of glass-fiber reinforced thermoplastic materials under high strain rates. *Polymer Testing*, *27*, 893–900. https://doi.org/10.1016/j.polymertesting.2008.07.006

Soutis, C. (2015). Introduction: Engineering Requirements for Aerospace Composite Materials. In P. E. Irving & C. Soutis (Eds.), *Polymer Composites in the Aerospace Industry* (pp. 1–18). Cambridge: Elsevier Ltd. https://doi.org/10.1016/B978-0-85709-523-7.00002-5

Staab, G. H. (2015). *Laminar Composites* (Second Edi). Boston: Elsevier Inc.

TenCate. (2016). TenCate Cetex and CFRT Thermoplastic Advanced Composites. Retrieved from http://www.tencate.com/advancedcomposites/products/thermoplastic/default.aspx

Todo, M., Takahashi, K., Béguelin, P., & Kausch, H. H. (2000). Strain-rate dependence of the tensile fracture behaviour of woven-cloth reinforced polyamide composites. *Composites Science and Technology*, *60*, 763–771. https://doi.org/10.1016/S0266-3538(99)00184-0

Vodicka, R. (1996). *Thermoplastics for Airframe Applications A Review of the Properies and Repair Methods for Thermoplastic Composites*. Melbourne.

Weeks, C. A., & Sun, C. T. (1998). Modeling Non-Linear Rate-Dependent Behavior in Fiber-Reinforced Composites. *Composites Science and Technology*, *58*, 603–611.

6. RESPONSIBILITY NOTICE

The authors are the only responsible for the printed material included in this paper.